Annals of Botany **116**: 261–277, 2015
doi:10.1093/aob/mcv092, available online at www.aob.oxfordjournals.org

ANNALS OF BOTANY
Founded 1887

Modelling and predicting the spatial distribution of tree root density in heterogeneous forest ecosystems

Zhun Mao[1,2]*, Laurent Saint-André[3,5], Franck Bourrier[1,2], Alexia Stokes[4] and Thomas Cordonnier[1,2]

[1]IRSTEA, UR EMGR, Centre de Grenoble, 2 Rue de la Papeterie, BP 76, 38402 Saint-Martin-d'Hères Cedex, France, [2]Université Grenoble Alpes (UGA), 38402 Grenoble, France, [3]INRA, UR BEF – Biogéochimie des Ecosystèmes Forestiers, 54280 Champenoux, France, [4]INRA, UMR AMAP, Boulevard de la Lironde, 34398 Montpellier Cedex 5, France and [5]CIRAD, UMR Eco&Sols, place Viala, 34398 Montpellier Cedex 5, France
** For correspondence. E-mail maozhun04@126.com*

Received: 27 March 2015 Returned for revision: 15 April 2015 Accepted: 7 May 2015 Published electronically: 14 July 2015

• **Background and Aims** In mountain ecosystems, predicting root density in three dimensions (3-D) is highly challenging due to the spatial heterogeneity of forest communities. This study presents a simple and semi-mechanistic model, named ChaMRoots, that predicts root interception density (RID, number of roots m^{-2}). ChaMRoots hypothesizes that RID at a given point is affected by the presence of roots from surrounding trees forming a polygon shape.
• **Methods** The model comprises three sub-models for predicting: (1) the spatial heterogeneity – RID of the finest roots in the top soil layer as a function of tree basal area at breast height, and the distance between the tree and a given point; (2) the diameter spectrum – the distribution of RID as a function of root diameter up to 50 mm thick; and (3) the vertical profile – the distribution of RID as a function of soil depth. The RID data used for fitting in the model were measured in two uneven-aged mountain forest ecosystems in the French Alps. These sites differ in tree density and species composition.
• **Key Results** In general, the validation of each sub-model indicated that all sub-models of ChaMRoots had good fits. The model achieved a highly satisfactory compromise between the number of aerial input parameters and the fit to the observed data.
• **Conclusions** The semi-mechanistic ChaMRoots model focuses on the spatial distribution of root density at the tree cluster scale, in contrast to the majority of published root models, which function at the level of the individual. Based on easy-to-measure characteristics, simple forest inventory protocols and three sub-models, it achieves a good compromise between the complexity of the case study area and that of the global model structure. ChaMRoots can be easily coupled with spatially explicit individual-based forest dynamics models and thus provides a highly transferable approach for modelling 3-D root spatial distribution in complex forest ecosystems.

Key words: Heterogeneous forest ecosystems, plant growth modelling, tree root density, fine root, coarse root, root system architecture, logistic function, Weibull distribution, log-normal distribution, Gompertz distribution, *Abies alba*, silver fir, *Picea abies*, Norway spruce.

INTRODUCTION

Tree roots can constitute >60 % of total biomass in forest ecosystems (Vogt *et al*., 1996). To evaluate below-ground ecosystem services, a reliable characterization of the spatial distribution of root density is fundamental. However, determining root density can be challenging, especially in remote locations or protected areas where root excavation is difficult or limited, e.g. at high altitudes or in naturally regenerated forests. These forests also possess particularly heterogeneous distributions of roots in both space and time (Soethe *et al*., 2006; Schwarz *et al*., 2010; Mao *et al*., 2012, 2013), and therefore reliable data remain scarce. Developing an accurate model that could predict root density from above-ground tree dimensions would be highly useful in complex forest ecosystems and could likely be applied to other types of forest.

In naturally regenerated montane and subalpine forests, trees commonly grow in clusters named tree islands, i.e. canopy-closed zones surrounded by clusters of trees. Between the clusters are gaps, i.e. canopy-open zones (Mao *et al*., 2012). In each cluster there is usually more than one species, tree ages are different and there is an irregular distribution of tree locations. Soil is also spatially heterogeneous, due, for example, to a high presence of stones that can obstruct root extension. Root growth of trees might also be in competition with that of shrubby and herbaceous understorey plants, rendering more difficult the modelling of root density distribution.

Models of tree root spatial distribution have been developed for the last 40 years (Böhm, 1979; Coutts, 1983; Schenk and Jackson, 2002; Zianis *et al*., 2005; Picard *et al*., 2012). The distribution of root density, either horizontal (e.g. along a gradient of canopy openness) or vertical (e.g. along a gradient of soil depth), is supposed largely to be a consequence of intrinsic and ontogenic traits and environmental factors (Picard *et al*., 2012). Different tree species possess different root system

architectures, which change throughout the life of a tree. Environmental factors affecting root density distribution can be (1) abiotic, including climatic, e.g. altitudinal trends (Hertel and Schöling, 2011; Mao *et al*., 2015), edaphic, e.g. water and nutrient availability in soil (Coutts *et al*., 1999), soil texture and compaction level (Dexter, 2004) and topographic, e.g. the presence of physical obstructions such as stones (Hoffmann and Usoltsev, 2001; Soethe *et al*., 2006) and slope angle (Di Iorio *et al*., 2005; Chiatante and Scippa, 2006), and (2) biotic, e.g. interactions between trees and between trees and understorey species (van Noordwijk *et al*., 1996; Cardinael *et al*., 2015). Existing models have been developed on the basis of the above sources of effects. Most models are allometric relationship-based (ARB) models, in which root density varies as a function of dendrometric properties of aerial tree organs and spatial distance [horizontal and/or vertical (for reviews see Hoffmann and Usoltsev, 2001; Schenk and Jackson, 2002; Zianis *et al*., 2005; Day *et al*., 2010)]. The ARB models generally have a simple and empirical structure and a small number of easy-to-measure parameters, and thus are easy to operate. However, most ARB models are developed at the scale of the plant individual and do not take into account the effects of interactions between trees. Thus, the relevance of up-scaling and applying tree individual-based ARB models to the whole-forest scale remains questionable, especially for heterogeneous mountain forests.

Another group of models developed at the plant individual scale aims at simulating spatio-temporal root growth dynamics. These models can be either (1) pseudoroot system architecture (RSA) models, which simulate the spatio-temporal distribution details of root density in a given soil volume as a proxy of RSA via diffusion or carbon allocation processes (Mulia *et al*., 2010), or (2) true RSA models, which simulate RSA skeletons via stochastic approaches (Doussan *et al*., 2003). Compared with ARB models, both pseudo-RSA and true RSA models are more sophisticated because they are more mechanistic, considering both root proliferation and certain biological parameters. The RSA models are more dynamic in time and space (i.e. root growth can be integrated) and can simulate two-dimensional (2-D) or three dimensional (3-D) root architecture skeletons or proxies of RSA that are highly realistic. Such models also have a strong potential to take into account interactions between trees (Pagès *et al*., 2004) and between trees and understorey species (Collet *et al*., 2006), although most RSA models have not considered these interactions yet. Nevertheless, the existing RSA models are mostly designed for agricultural crops or agroforest trees, which constitute relatively regular and homogeneous ecosystems in both above- and below-ground compartments (Mulia *et al*., 2010). Thus, the applicability of RSA models to naturally regenerated trees within highly heterogeneous mountain ecosystems remains uncertain. Furthermore, most models require many complex parameters related to root traits and development. These parameters are either unavailable for natural species or are time-consuming to estimate.

High-altitude, mixed, naturally regenerated forest ecosystems are complex in vegetation distribution and environmental conditions and therefore new models for predicting the spatial distribution of root density are needed. It is preferable that these models possess the advantages of both ARB and RSA approaches and comprise simple equations with easy-to-measure inputs for forest and environmental characteristics. Models should also combine mechanistic processes and ecologically meaningful parameters. It is also desirable that model predictions are spatially explicit and can be used for up-scaling. Such models are lacking, especially for highly heterogeneous forest ecosystems. Nevertheless, some modelling studies on root distribution exist (Gersani *et al*., 2001; Müller and Wagner, 2003; Roering *et al*., 2003; O'Brien *et al*., 2007), as they are simple and include plant interactions. For example, Müller and Wagner (2003) and Roering *et al*. (2003) developed models whereby they hypothesized that root density at a given point was affected by the presence of roots from the surrounding trees and that density varied between this point and the tree stem. On the basis of game theory, Gersani *et al*. (2001) and O'Brien *et al*. (2007) considered that a plant produces fewer roots when in competition with its neighbour than if it is isolated. Root overlapping was also taken into account. These models appear suitable to capture some features of complex forest stands (e.g. spatial heterogeneity of trees and tree interactions), although several were not initially developed for modelling forest ecosystems (e.g. Gersani *et al*., 2001; O'Brien *et al*., 2007).

We developed a model based on the hypothesis that root density at a given point is affected by the presence of roots of surrounding trees forming a polygon shape, with a possible saturating effect depending on the total density of surrounding trees. The effect of tree size and distance to a given point, species, presence of rocks and competition with roots of the understorey vegetation was investigated. Data to test the model were collected in the French Alps. The root density indicator was root interception density (RID, number of roots m^{-2}), which is one of the most commonly used root indicators characterizing root density (Van Noordwijk *et al*., 2000; Maurice *et al*., 2010; Mao *et al*., 2012, 2013). RID can be used in the calculation of root area ratio (i.e. total root cross-sectional area per soil area) and is a key input for assessing the role of roots in reinforcing soils against shallow landslides (Stokes *et al*., 2009; Mao *et al*., 2012, 2013). RID is also considered a suitable proxy to evaluate above- and below-ground carbon allocation at a stand level (Mao *et al*., 2015). As RID is easy to measure, it has been frequently used for estimating root length density (RLD) (Van Noordwijk *et al*., 2000; Chopart *et al*., 2008; Maurice *et al*., 2010; Cardinael *et al*., 2015). Root length density is often used as a proxy to characterize plant water and nutrition uptakes in forest or agricultural systems (Chopart *et al*., 2008). The potential of our model is discussed with regard to its more widespread use in several types of forest ecosystems.

MATERIALS AND METHODS

Description of the model

The model, called ChaMRoots (Characterisation of Mountain forest Roots) comprises three sub-models for predicting the following parameters (Note: according to the international standard ISO 31–11, $]x, y]$ denotes a left half-open interval from x (excluded) to y (included)):

1. Spatial heterogeneity of tree roots. The sub-model predicts the RID of roots]0, 1] mm in diameter within the top 0·2 m of soil as a function of tree species, tree dimension [e.g. basal area at breast height (g)], tree position [i.e. the

distance between the tree and a given point (D)] and the presence/absence of obstacles (e.g. stones) in soil that emerge on the ground (O).
2. Diameter spectrum. The distribution of RID as a function of root diameter class for roots $\geq$1 mm in diameter is predicted by the second sub-model.
3. Vertical profile. The vertical distribution of RID as a function of soil depth (z) is predicted by the third sub-model.

Sub-model of spatial heterogeneity of tree roots The fundamental principle of the first sub-model is that a tree contributes more to total root density at a given point when it is large, close to that point and no obstacles are present between the tree and the given point. The higher potential production of roots also depends on species and site conditions. The contribution of roots to total density is implicitly modulated by the presence of other trees due to inter-tree competition. Distance, tree size, obstacles and species were therefore selected as the main factors influencing tree root density (Hoffmann and Usoltsev, 2001).

The core of the first sub-model of root spatial heterogeneity is based upon root production efficiency (E) at a given point, which depends on the surrounding trees. E is defined by:

$$E = \frac{\mathrm{d}RID_{t,0-1}}{\mathrm{d}p} \tag{1}$$

where p is the potential of trees to grow roots at a given point in the soil. The term 'tree root potential' or p will be used hereafter. The value of p depends on the dimension and position of the surrounding trees. p differs from E, which measures the capacity of trees to convert a unit of p to root density. $RID_{t,0-1}$ is the RID of the finest tree roots; $\mathrm{d}RID_{t,0-1}/\mathrm{d}p$ is the production of $RID_{t,0-1}$ per p metric.

p at a given point is defined by the following general form:

$$p = \sum_{s}^{N_s}\sum_{e}^{N_e} p_{e,s} = \sum_{s}^{N_s}\left(\sum_{e}^{N_e} \frac{g_{e,s}^{\lambda_s}}{\beta + (D_{e,s}^{\alpha})^{\varphi_s}} O_{e,s}\right) \tag{2}$$

N_s is the number of tree species around the target point ($N_s \geq 0$, $s \in [0, N_s]$). N_e is the number of tree individuals of a given species s around the target point ($N_e \geq 0$, $e \in [0, N_e]$). $p_{e,s}$ is the tree root potential contributed by a tree (e, s). $g_{e,s}$ is the basal area at a height of 1·3 m of an individual tree e of species s (m^2). $D_{e,s}$ is the horizontal distance from the centre of a tree (e, s) to the target point (m) and has a value $\geq$0. $O_{e,s}$ is the absence of emerged obstacles (diameter $>\sim$30 cm) on the ground between the target point and tree e of species s. The value of $O_{e,s}$ can be either binary (1 = yes, absence of obstacles; 0 = no, presence of obstacles) or unique (1 = yes, indifferent to the absence or presence of obstacles), depending whether the effect of obstacles is considered. α and β are scaling parameters of the surrounding trees' influence on p, while λ_s and φ_s are RSA parameters (see below). These four parameters are fitted parameters.

α and β are generic coefficients (α and $\beta \geq$0) accounting for the effect of intrinsic tree allometry regardless of tree species, as they allow an alteration of the weight of $D_{e,s}$ relative to $g_{e,s}$. When $\beta = 0$, both $p_{e,s}$ and $p \in [0, +\infty[$, if $D_{e,s}$ tends to approach 0, i.e. the given point is situated at the centre of the tree (e, s), then p tends to infinity. When $\beta > 0$, β is effectively limiting the ratio between g_i and D_i, without the drawback of pulling $p_{e,s}$ towards infinity. To estimate α and β, we tested the following cases:

1. $\alpha, \beta \in [0, +\infty[$
2. $\alpha \in [0, +\infty[$, $\beta = 0$
3. $\alpha \in [0, +\infty[$, $\beta = 1$

λ_s and φ_s are specific coefficients (λ_s, $\varphi_s \geq 0$) accounting for the effect of RSA. Species that differ in architecture may possess variable capacities for root extension, which results in a disparity in the spatial distribution of roots in the soil. We divided species into three groups according to the morphology of the root system, using the classification of Köstler *et al*. (1968), as follows.

1. Plate-like morphology, with a greater superficial, horizontal root extension compared with that of the vertical roots, e.g. *Picea abies*. In this case, $\lambda_s = \lambda_p$, $\varphi_s = \varphi_p$.
2. Taproot morphology ($\lambda_s = \lambda_a$), with a greater extension of vertical roots compared with the extension of horizontal and lateral roots, e.g. *Abies alba*. In this case, $\lambda_s = \lambda_a$, $\varphi_s = \varphi_a$.
3. Heart-like morphology, where the root system is a mixture of the above two types, e.g. *Fagus sylvatica*, *Sorbus aucuparia*, *Acer pseudoplatanus*. In this case, $\lambda_s = \lambda_b$, $\varphi_s = \varphi_b$.

To facilitate the estimation of coefficients, we consider *P. abies* as the reference species and let $\lambda_p = 1$ and $\varphi_p = 1$. The p of *A. alba* and broadleaves based on λ_a, φ_a and λ_b φ_b can be considered as relative p compared with *P. abies*. In this study, due to a small population of broadleaves, p_b was forced to share the same coefficient with either p_p or p_a, i.e. $N_s = 2$. The following two cases were tested:

1. $\lambda_p = 1$; $\varphi_p = 1$; $\lambda_a = \lambda_b \in [0, +\infty[$, $\varphi_a = \varphi_b \in [0, +\infty[$
2. $\lambda_p = \lambda_b = 1$, $\varphi_p = \varphi_b = 1$, $\lambda_a \in [0, +\infty[$, $\varphi_a \in [0, +\infty[$

where broadleaves were grouped together with *A. alba* and *P. abies*, respectively.

To estimate λ_s and φ_s, we tested the following cases:

1. $\lambda_s \in [0, +\infty[$, $\varphi_s = 1$
2. $\lambda_s = 1$, $\varphi_s \in [0, +\infty[$
3. $\lambda_s \in [0, +\infty[$, $\varphi_s \in [0, +\infty[$, $\lambda_s = \varphi_s$

These three cases represent different biological phenomena concerning the effect of species on tree root extension. Options (1) and (2) assume that the effect of species on p is uniquely effective with regard to tree size and the distance between the tree and the target point, respectively; while (3) assumes that the effect of species on p is effective with regard to $g_{e,s}$ and $D_{e,s}{}^{\alpha}$, i.e. both tree size and position.

We modelled E using two approaches. Firstly, in a semi-mechanistic approach, E was assumed to be dependent on two factors: (1) the 'root-providing pool', which represents the existing quantity of roots from which the finest roots can be borne; (2) the 'restraining pool', representing the upper limit of the finest root production due to root competition, which can be

both intra- and inter-species specific. Therefore, E can be written as a derived form of the logistic function:

$$E = rRID_{t,x-y}\left(1 - \frac{RID_{t,0-1}}{K} - \theta\frac{RID_{u,0-1}}{K}\right) \quad (3)$$

Here, K is the maximum density of RID_{0-1} of both tree and understorey species that the soil can support, $RID_{u,0-1}$ is the RID of understorey species and θ is the coefficient describing the relationship between understorey species' roots and tree roots. If $\theta = 0$, there is a neutral relationship of root growth between tree and understorey species, and E is uniquely determined by the RID of the trees. If $\theta > 0$, understorey species' roots are in competition with tree roots; for a given K, a higher θ value reflects a greater detrimental effect of understorey species' roots on tree roots. Theoretically, θ can be negative, suggesting that roots of understorey species are in a mutualistic relationship with tree roots, but this phenomenon might be rarely observed in reality. r is the average branching rate for the production of RID_{0-1}, and $RID_{t,x-y}$ is the RID of tree roots in the class of root diameter]x, y] mm from which fine roots can be borne.

Preliminary regression analyses based on our monolith data (see section Tree and root data) revealed that $RID_{u,0-1}$ had no significant effect on $RID_{t,0-1}$ ($P > 0{\cdot}40$, data not shown), suggesting a low competitive effect between understorey species' roots and tree roots in our study sites. Hence, we set $\theta = 0$, simplifying eqn (3) by removing the non-significant interactions between RID of trees and that of the understorey species:

$$E = rRID_{t,x}\left(1 - \frac{RID_{t,0-1}}{K_t}\right) \quad (4)$$

where K in eqn (4) is replaced by K_t, which denotes the maximum density of RID_{0-1} of tree roots.

Field observations from rhizotrons at the same field sites showed that roots]0, 1] mm in diameter could be branches initiated on roots of]1, 5] mm or those of]0, 1] mm (Mao *et al.*, 2013). Hence, we have:

$$RID_{t,x-y} = RID_{t,0-5} = \mathrm{RID}_{t,0-1} + RID_{t,1-5} \quad (5)$$

Here we chose to use a linear relationship between $RID_{t,1-5}$ and $RID_{t,0-1}$ regardless of site rather than non-linear curves or fitting one curve per site, as a linear relationship leads to a more simple integral equation, i.e. eqn (5).

$$RID_{t,1-5} = a\ RID_{t,0-1} + b \quad (6)$$

where a and b are the slope and intercept coefficients of the linear univariate equation $a \geq 0$; $b > 0$.

By linking eqns (1), (5) and (6), the integrated form of eqn (4) (see Supplementary Data S1 for details of deduction) is:

$$RID_{t,0-1} = \frac{b\ (U-1)}{1 + a + bU/K_t} \quad (7a)$$

where:

$$U = e^{(1+a+b/K_t)rp} \quad (7b)$$

According to eqns (7a) and (7b), we see that when $p = 0$ (no tree), $RID_{t,0-1} = 0$, and when $p \to +\infty$ (no limitation of the maximum tree inclusion zone), $RID_{t,0-1} \to K_t$.

Alternatively, we modelled E and $RID_{t,0-1}$ in an empirical approach using a power function, which is one of the most commonly attempted functions when exploring a relationship between two variables:

$$E = (mn)p^{n-1} \quad (8)$$

$$RID_{t,0-1} = mp^n \quad (9)$$

where m and n are the two coefficients of the power function. Such a comparison allowed us to discuss the efficiency of different approaches.

Sub-model of diameter spectrum. We modelled the cumulative frequency C_d (dimensionless) of RID as a function of the upper boundary of root diameter class (d). Compared with absolute values of RID, C_d enabled us to reduce the irregular jump of data points from one diameter class to another. We tested four types of function for the optimum fit of the sub-model of diameter spectrum, including a one-parameter cumulative distribution function (CDF) of exponential distribution [eqn (10a), 'exponential']:

$$C_d = 1 - e^{-\zeta d} \quad (10a)$$

and three two-parameter functions, i.e. a Weibull distribution [eqn (10b), 'Weibull'], Gompertz distribution [eqn (10c), 'Gompertz'] and log-normal distribution [eqn (10d), 'log normal'], respectively:

$$C_d = 1 - e^{-(d/\gamma)^{\kappa}} \quad (10b)$$

$$C_d = 1 - \exp\left[-\frac{\eta}{\delta}\left(e^{\delta d} - 1\right)\right] \quad (10c)$$

$$C_d = \frac{1}{2}\left[1 + \mathrm{erf}\left(\frac{\ln d - \mu}{\sigma\sqrt{2}}\right)\right] \quad (10d)$$

where C_d is the cumulative frequency of RID from the finest roots to those of root class diameter d mm (dimensionless), $d \in$]0, 50] mm; $C_d \in [0, 1]$, ζ, γ, κ, η, δ, μ and σ are the coefficients of root of diameter spectrum in the CDFs, and erf is the Gauss error function.

Sub-model of vertical profile. Root density varies significantly with soil depth, which has, in turn, commonly been used as a key parameter when modelling vertical root distribution (Gale and Grigal, 1987; King *et al.*, 2003). To facilitate comparison with previous studies, we modelled the root distribution along a vertical soil profile using the following one-parameter exponential model:

$$C_z = 1 - \varepsilon^{100z/z_{\max}} \quad (11)$$

where C_z is the cumulative frequency of RID from ground surface to the soil depth z (m); $C_z \in [0, 1{\cdot}0]$, with $z \in$]0, $z_{\max}$] and

ε is the coefficient of root profile shape, with $\varepsilon \in [0, 1[$. The closer ε approaches 1, the more roots tend to be less concentrated at the soil surface. We fixed maximum soil depth at 1·0 m according to field observations from the same field site (Mao *et al*., 2013). This equation is derived from the model of Gale and Grigal (1987) for estimating the vertical distribution of roots.

Tree and root data

Characteristics of study sites. Our study sites were located near the village of Chamrousse, Isère, France (45°07'7N, 5°52' E) and comprised two mixed, mature, naturally regenerated forests of Norway spruce (*P. abies*), silver fir (*A. alba*) and European beech (*F. sylvatica*) growing at altitudes of 1400 m a.s.l. (Prémol forest) and 1700 m a.s.l. (Bachat-Bouloud forest). Mean monthly air temperature was lowest in January or February (–5·2 °C at 1400 m, –3·6 °C at 1700 m) and highest in July (13·7 °C at 1400 m, 12·0 °C at 1700 m). Average annual precipitation is 1530 mm at 1400 m and 1710 mm at 1700 m. Soils are acidic at both sites. According to the World Reference Base (IUSS Working Group WRB, 2007) for soil resources, the soil is classified as Cambisols (Hyperdystric) at Prémol and as Cambisols (Humic, Hyperdystric) at Bachat-Bouloud. A high presence of coarse elements (rocks and stones) was found at both sites. More details about the site characteristics are available in Mao *et al*. (2012).

Plot settings for tree and root data. Two 25 m × 25 m plots were set at each site for forest inventories, except for one plot at 1400 m, which was 25 m × 30 m. Within each plot, two locations were randomly selected for excavating roots: one in a tree island and the other in a tree gap (see Fig. 1 for examples of trench location within two chosen plots). Each root trench had a dimension of 1·0 m (length) × 0·6 m (width) × 1·0 m (depth, i.e. maximum rooting depth). Sets of data on forest inventories for global site descriptions and those for root density and growth dynamics in each trench are available in Mao *et al*. (2012, 2013).

At each site, one of the two plots was chosen for mini-monolith excavation. Mini-monoliths were systematically distributed on the edge and diagonal of the plots (Fig. 1) with two exceptions: no mini-monolith was excavated at point O at Prémol or at point J at Bachat-Bouloud, as their locations were disturbed by an earlier excavation for rhizotron installation and root sampling in the summer of 2009 (Mao *et al*., 2013). A new point P at Prémol was selected randomly in the same plot. As a result, we obtained 25 mini-monoliths in all: 13 at Prémol and 12 at Bachat-Bouloud. Each mini-monolith had a dimension of 0·2 m (length) × 0·2 m (width) × 0·2–0·3 m (depth).

Tree measurement and eligibility of 'visible trees'. Within each plot, species name, diameter at breast height (DBH) and location of all the trees were registered during a forest inventory in September 2009 (Mao *et al*., 2012). In the spring of 2010, a second forest inventory was conducted. From the location of a mini-monolith, species name, DBH, azimuth and distance of each visible tree in any direction (0° to 360°), were registered within a radius of 10·0 m. Figure 1 shows the mapping of trees for both inventories in the two plots.

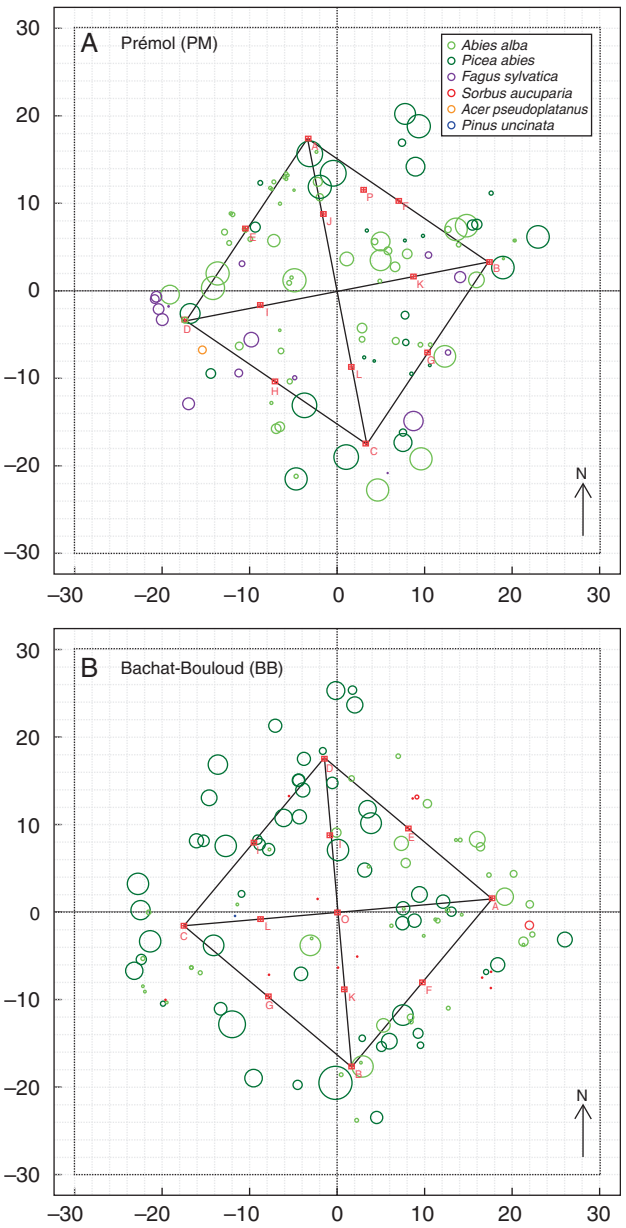

FIG. 1. Mapping of mini-monoliths (squares) and tree trunks of different species (circles of different colours) based on forest inventories in 2009 and 2010. *x*- and *y*-axes are distances in metres. The diameter of each tree trunk has been enlarged five times for easier viewing.

At each mini-monolith, two values of the maximum tree inclusion zone (MIZ) were tested: MIZ = 8·0 m and MIZ = 10·0 m. Within the MIZ of each mini-monolith, a tree is considered visible if the centre of the trunk is not eclipsed by the trunk of any other visible trees. A visible tree can be either inside or outside the plot of 25 × 25 m^2. For each monolith, only visible trees are assumed to be effective in influencing root density. A detailed protocol of visible tree selection and the outcomes of mapping at each sampling point are available in Supplementary Data S2.

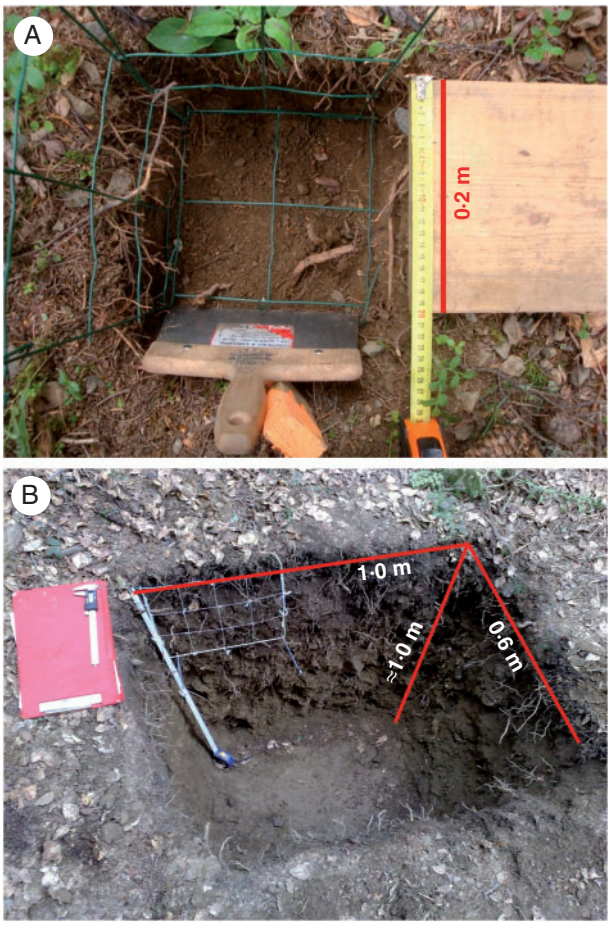

FIG. 2. Measurement of root interception density using (A) mini-monolith and (B) soil trenching techniques.

Root data from mini-monoliths. Root sampling in mini-monoliths (Fig. 2A) was carried out in the summer of 2010. For each mini-monolith, we gave a qualitative description of the location of the point with regard to tree canopies [three levels: outside, transitional (i.e. on the edge of canopies) and inside] and the absence of emerged obstacles (mainly rocks of diameter >0·5 m) between the point and each of the surrounding trees (two levels: 1 = yes, absence of obstacles; 0 = no, presence of obstacles). Root excavation was strictly limited within a zone of 0·2 m × 0·2 m. Soil was carefully removed by hand and sometimes using a long nail if rocks were present. Roots connected to the soil to remove and on the lateral walls were cut using either scissors (for thin and fibrous roots) or secateurs (for coarse and highly lignified roots) so as to avoid ripping roots from the lateral soil profiles. Finally, root tips were counted on the soil profiles, layer by layer, using a metal grid with a square unit of 0·1 m × 0·1 m. RID is always associated with the angle of the soil profile and hence can be measured on a vertical, horizontal or oblique soil profile. In this study, only RID on the lateral soil profiles, i.e. walls perpendicular to the ground surface, were shown and used for model fitting, as lateral soil profiles are one of the most conventional and representative cases of root sampling (Böhm, 1979). All roots (regardless of species) were counted and classed into seven different categories of diameter:]0, 1],]1, 2],]2, 3],]3, 5],]5, 10],]10, 20] and]20, 50] mm. We assumed that the counted roots contained mostly living roots, as decomposed or dead roots usually dropped from the soil profile surface during excavation. Plant functional groups (trees and shrubby and herbaceous species; the latter two are considered understorey species) were distinguished for roots >1 mm in diameter. For root intercepts of]0, 1] mm in diameter, the plant functional group was difficult to identify *in situ* due to the presence of a variety of understorey species at both sites. Therefore, we estimated the RLD of roots that were simultaneously collected from the mini-monoliths, then washed in the laboratory, sorted according to functional group, scanned and analysed using the software WINRHIZO® (Regent Inc., Canada). In the laboratory, the functional group to which a root belonged was identified by its colour, texture and smell. To separate the RID of trees from understorey species, we assumed:

$$P_{u,0-1} = \frac{100\ \widehat{RID}_{u,0-1}}{\widehat{RID}_{u,0-1} + \widehat{RID}_{t,0-1}} = \frac{100\ RLD_{u,0-1}}{RLD_{u,0-1} + RLD_{t,0-1}} \quad (12a)$$

$$P_{t,0-1} = \frac{100\ \widehat{RID}_{t,0-1}}{\widehat{RID}_{u,0-1} + \widehat{RID}_{t,0-1}} = \frac{100\ RLD_{t,0-1}}{RLD_{u,0-1} + RLD_{t,0-1}} \quad (12b)$$

P_u is the percentage of total root density of understorey species. P_t is the percentage of total root density of tree species, with $P_t = 100 - P_u$. $\widehat{RID}$ is the estimated RID based on the RLD data. *RLD* is the measured RLD from WINRHIZO® analysis. The subscripts (t,0–1) and (u,0–1) of the indicators denote roots of]0, 1] mm in diameter from tree and understorey species (number of roots m^{-2}), respectively.

Root data from trenches. The RID data based on measurements using trenches (Fig. 2B) of 1·0 m (length) × 0·6 m (width) × 1·0 m (depth) in Mao *et al.* (2012) were determined in the summer of 2009. Four trenches were dug at each site. Within each trench, root distribution was measured along each soil profile. Therefore, there were 16 sections in total and eight sections per site (Mao *et al.*, 2012). On each profile wall, root intercepts were counted using the same protocol as for mini-monoliths, except that the root diameter class]2, 5] mm was used instead of the classes]2, 3] and]3, 5] mm used in the mini-monoliths. Plant functional groups were not distinguished. Since we measured neither the RID of tree species nor that of understorey species in any trenches, we used the average values of P_u and P_t of the mini-monoliths, which were classified as 'inside the tree canopies' and 'outside the tree canopies', towards trenches in tree islands and gaps, respectively:

$$\begin{aligned} P_{TI,t,x-y} &= 100 - P_{TI,u,x-y} \\ &= \left(\sum_{n=1}^{N_{\text{inside}}} \frac{100\ RID_{n,t,x-y}}{RID_{n,u,x-y} + RID_{n,t,x-y}} \right) / N_{\text{inside}} \end{aligned} \quad (13a)$$

$$\begin{aligned} P_{G,t,x-y} &= 100 - P_{G,u,x-y} \\ &= \left(\sum_{n=1}^{N_{\text{outside}}} \frac{100\ RID_{n,t,x-y}}{RID_{n,u,x-y} + RID_{n,t,x-y}} \right) / N_{\text{outside}} \end{aligned} \quad (13b)$$

where P_{TI} and P_G are the percentages of density of roots]x, y] mm in diameter from species in islands and gaps,

TABLE 1. *Mean and standard deviation (s.d.) of percentages of roots from tree species (P_t, %), estimated using root interception density data from mini-monoliths*

Site	Location with regard to tree canopies	Percentage of roots from tree species (P_t)					
		]0, 1] mm		]1, 2] mm		]2, 5] mm	
		Mean	s.d.	Mean	s.d.	Mean	s.d.
Bachat-Bouloud	Outside	24·5	9·2	72·7	19·8	85·4	22·6
	Transitional	34·4	11·4	45·3	21·8	73·7	29·7
	Inside	60·0	17·4	95·2	9·5	98·4	3·2
Prémol	Outside	13·6	13·9	76·9	22·1	86·7	18·9
	Transitional	48·1	35·3	94·2	8·0	95·3	6·6
	Inside	78·5	19.7	86·0	19·4	96·6	4·9

For root diameter]0, 1] mm, P_t was estimated using root WINRHIZO®, which measured root length density of each type of functional group, as it was impossible to identify to which functional group a root tip belonged. See also Mao *et al*. (2015).

respectively. N_{inside} and N_{outside} are the total numbers of mini-monoliths situated inside and outside tree canopies. Subscript n is the sequence of mini-monolith, with $n \in N_{\text{inside}}$ *or* N_{outside}; *TI* is tree islands; subscript G is gaps and subscripts x and y are the lower and upper limits of a class of root diameter]x, y] mm.

Based on eqns (13a) and (13b), estimates of P_t for tree islands and gaps at two sites are available (Table 1). As no roots of]5, 50] mm in diameter were identified as being from understorey species, we assumed $P_t = 100$ % and $P_u = 0$ % for these root diameter classes.

2.3 Statistical modelling

Data from mini-monoliths ($N_f = 25$, where N_f is the number of observations for model fit) were used to fit the sub-model of spatial heterogeneity and that of diameter spectrum for roots within a soil depth of]0·0, 0·2] m. Beyond this depth, i.e. for the depth of]0·2, 1·0] m, the data from root trenches were used to fit the sub-model of diameter spectrum ($N_f = 16$). Since the roots were measured to the maximum rooting depth at each site, these root data were also used to fit the sub-model of vertical profile ($N_f = 16$). To choose the optimal sub-models, we calculated (1) root mean square error:

$$\text{RMSE} = \sqrt{\left[\sum_{i=1}^{N_f} (\widehat{Y}_i - Y_i)^2\right] / N_f} \qquad (14)$$

where $\widehat{Y}_i$ and Y_i are the predicted and observed values; $i \in [1, N_f]$, (2) the Akaike information criterion (AIC), (3) the Bayesian information criterion (BIC) and (4) the coefficient of determination (R^2, dimensionless) as quantitative indicators (Burnham and Anderson, 2002).

All the sub-models were validated using root data that were not used for model fitting. The sub-model of spatial heterogeneity was validated using the database from root trenches within a soil layer of]0·0, 0·2] m, in which $RID_{t,0-1}$ of four sections within one root trench were averaged ($N_v = 8$, where N_v is the number of observations for model validation). Regarding the sub-model of diameter spectrum and that of the vertical profile, only three sections out of four per root trench were chosen for fitting and the remaining one was used for model validation ($N_v = 8$). Statistical analyses were performed using R 2.13.0 (www.r-project.org).

RESULTS

Spatial heterogeneity

$RID_{t,1-5}$ significantly correlated with $RID_{t,0-1}$ at a soil depth of 0·2 m (Fig. 3). $RID_{t,1-5}$ was significantly higher at the Bachat-Bouloud site compared with Prémol for the same $RID_{t,0-1}$ (Fig. 3). Despite this significant site effect, occurring mainly on the intercept (b), we calibrated one slope (a) and one intercept (b) for both sites combined, to facilitate fits of eqns (10a) and (10b), instead of one pair of a and b per site, as the fit per site did not significantly improve R^2 (0·34 for Prémol and 0·43 for Bachat-Bouloud) compared with the fit for both sites combined (0·42). A higher number of sites, as well as a higher number of points per site, would have been necessary to better explore this effect.

Neither the effect of obstacle nor the choice of MIZ (8·0 versus 10·0 m) improved the fit regardless of fitting index (Fig. 4). Hence, the final sub-models chosen omitted O, but included MIZ = 8·0 m. Power function-based sub-models possessed significantly higher R^2 and lower RMSE, AIC and BIC than their homologous parameterization logistic function-based sub-models (Fig. 4). $RID_{t,0-1}$ within the soil layer]0·0, 0·2] mm significantly increased as a function of p, regardless of the parameterization on α, β, λ_s in eqn (2) (Fig. 5 and Supplementary Data S3).

We decided to select models having acceptable statistical index values and with all their parameters as significant. We selected one model per type of function (power versus logistic) because of the different ways that models were constructed. Both types of final sub-model selected, i.e. No. 2 for power function and No. 10 for logistic function, possessed exactly the same parameterisation of p (Supplementary Data S3). The most preferential structure for modelling p omitted the intercept β and kept the effect of species λ_s as effective at both nominator and denominator. The coefficient $\lambda_s > 1·0$ reflected the difference in RSA between the reference species *P. abies* and the other species. Despite the statistical significance, this effect remained less pronounced, with a value of λ_s close to 1·0

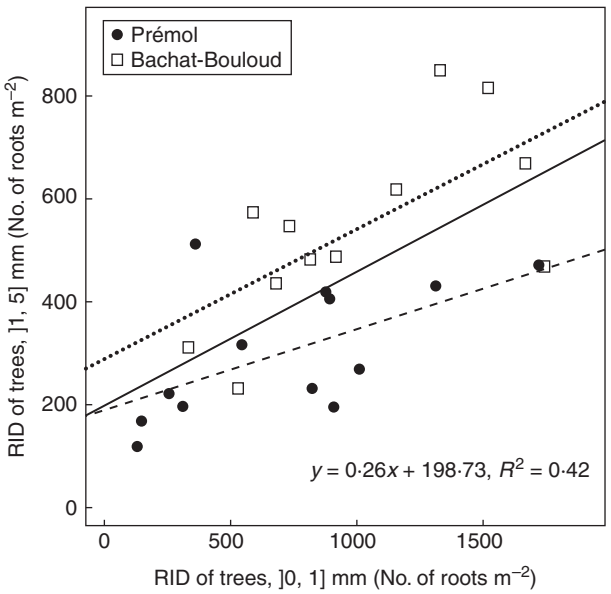

FIG. 3. Correlation between root interception density (RID) of]1, 5] mm and]0, 1] mm. Round symbols represent the Prémol site and square symbols the Bachat-Bouloud site. Solid, dashed and dotted lines denote the linear regressions for both sites (to which the equation refers), Prémol and Bachat-Bouloud, respectively.

(Table 2). Regrouping broadleaves together with *A. alba* slightly improved the models (Supplementary Data S3; number 9 versus 10 and number 1 versus 2).

Residuals were generally well distributed, although high dispersion was detected at low values of p, especially for the logistic function-based sub-model (Fig. 5). Compared with Prémol, the measured RID for Bachat-Bouloud tended to have a higher baseline. Thus, global sub-models for both sites underestimated $RID_{t,0–1}$ for Bachat-Bouloud and overestimated $RID_{t,0–1}$ for Prémol (Fig. 5). This result was more pronounced for the logistic function.

Diameter spectrum

The two-parameter functions (Weibull, Gompertz and log-normal CDF) exhibited significantly better fits than the one-parameter exponential CDF (Fig. 6A–D; Table 3, Zone I). Decomposing the MSE (square of RMSE) into fine and coarse roots, we observe that the lower performance of the exponential CDF fits the fine root data (Fig. 6E). With regard to the coarse roots, no significant deterioration of fit was found with the exponential CDF compared with the other functions.

Concerning the three two-parameter functions, the log-normal CDF usually performed better than the other functions when the soil depth was $<0{\cdot}8$ m. It appeared that the log-normal CDF was most frequently the best function (Table 3, Zone I). This suitability was mainly due to a better fit of this function for coarse roots (Table 3, Zone III). For fine roots, the log-normal CDF was not better than the Weibull or Gompertz CDF (Table 3, Zone II). The log-normal CDF fitted a 'round shoulder' type of diameter spectrum, with a gradual saturation of C_d when $\geq 0{\cdot}99$ (Fig. 7A). The Gompertz CDF was the best

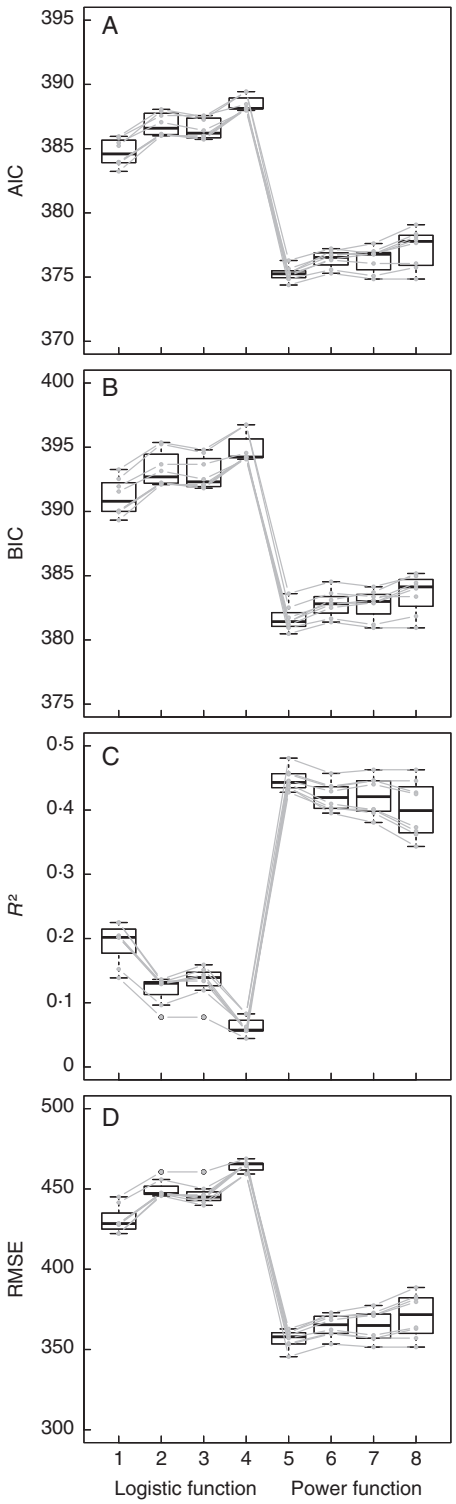

FIG. 4. Fitting comparisons between the sub-models of spatial heterogeneity in terms of the choice of MIZ (radius = 8·0 versus 10·0 m), consideration of the effect of obstacles (included versus excluded) and type of function (logistic versus power function). In each plot, eight boxplots are numbered from 1 to 8. Plots 1–4 refer to the logistic function and 5–8 to the power function; within each group of four boxplots, from left to right: MIZ = 8·0 × exclusion of the effect of obstacles (1 and 5); MIZ = 8·0 × inclusion of the effect of obstacles (2 and 6); MIZ = 10·0 × exclusion of the effect of obstacles (3 and 7); MIZ = 10·0 × inclusion of the effect of obstacles (4 and 8). Each grey line shows the tendency of each pattern of parameterization (β; regrouping of broadleaves; λ_s) corresponding to eqn (2).

function to fit the 'angular shoulder' type of diameter spectrum [i.e. C_d close to $\geq$0·99 up to the upper root diameter boundary (d) = 2 mm] or the 'shoulderless' type (i.e. C_d close to $\geq$0·99 until d = 1 mm) (Fig. 7B). Thus, the Gompertz and Weibull CDFs were more efficient in fitting the root diameter spectrum for deep depths, especially the layer]0·8, 1·0] m, where the diameter spectrum was mainly of the angular shoulder or shoulderless type. As a consequence, we advise the use of the log-normal CDF for predicting diameter spectrum when C_d is <0·99 for d = 1 mm and the Gompertz CDF for predicting diameter spectrum when C_d is $\geq$0·99 for d = 1 mm.

The two coefficients in both the log-normal and the Gompertz CDF exhibited significantly negative linear correlations and this result was more pronounced for the Gompertz CDF (Supplementary Data S3). Soil depth had a significant effect on the variation of the coefficients, but only σ showed a clear decreasing trend with soil depth (Supplementary Data S3).

Vertical profile

The increment in C_z decreased with increasing soil depth due to the lower root density at deeper soil layers. The quality of model fit deteriorated at higher root diameter classes, as R^2 tended to be more dispersed and smaller with increasing root diameter (Fig. 8A). Root diameter significantly affected the value of ε (Fig. 8B) and the shape of the vertical profile (Fig. 9). Coarse roots were more concentrated in shallow soil layers (Fig. 9C–F), which explains why ε was higher for fine roots (Fig. 8B). Variation in the curve shape was high within each of the root diameter classes and cannot be explained by either the effect of site or that of p (data not shown). When root diameter was $\leq$5 mm, curves of global model per root diameter class almost overlapped with those using median ε (Fig. 9A–C). When root diameter was >5 mm, global-model curves performed better than median-ε curves, as the former better approached the observed data (Fig. 9D–F). Therefore, we selected the six global models for each root diameter class, with their ε plotted in Fig. 8B.

Validation with non-fitted data

In general, the validation of each sub-model indicated that all sub-models of ChaMRoots had good fits (Supplementary Data S3). The sub-model of spatial heterogeneity had a more robust performance at higher p (Supplementary Data S3). For the sub-model of diameter spectrum, the preference for CDF (log-normal versus Gompertz) was well identified by soil depth. Despite a high level of data dispersion, diameter spectrum curves were quite evenly distributed at both sides of the predicted data when the log-normal CDF was used (Supplementary Data S3). The performance of the sub-model of vertical profile appeared ideal for roots in diameter classes]0, 1] and]1, 2] mm, but was less robust for the remaining root diameter classes (Supplementary Data S3).

DISCUSSION

Modelling algorithm for the first sub-model: spatial heterogeneity

The development of the parameter 'tree root potential', p, was highly relevant for the semi-mechanistic modelling of root distribution. RID increased with p in the top 20 cm of soil, thus demonstrating the validity of this approach. The use of p allowed us to adopt the classical approach used in previous ARB models, i.e. root density was based on both tree size and distance from the trunk. Additionally, p allowed us to take into account two sorts of biotic interaction between plants:

1. tree interception: roots at a given point are more influenced by immediate adjacent trees than by those at a distance. Despite the absence of hard data, ARB models focusing on an individual tree, support such a hypothesis, although they do not explicitly consider it at the forest scale.
2. root crossing: adjacent plants can extend and cross their roots in their shared soil environment (O'Brien *et al.*, 2007; Gao *et al.*, 2010).

Root crossing does not necessarily lead to a greater root density. In this study, we assumed that trees of the same species and size possess the same shape of p–distance curves. But trees close to each other might not have an increased root density at the mid-point between the trees, because of increased competition between roots for water and nutrients. For example, Ammer and Wagner (2002) found that root density of a single tree varies between closed and open canopies. In ChaMRoots, introducing the concept of production efficiency (E) avoids the over-estimation of root density for high values of p, because E declines with increasing p due to the presence of too many eligible individual trees. Therefore, the interaction between trees, although not explicitly considered in p, is implicitly involved in E. The conception of p and E in our study, especially the p and E based on the logistic function, is comparable with the metric G, i.e. plant individual fitness, in Gersani *et al.* (2001) and O'Brien *et al.* (2007). These authors hypothesized that tree root development is controlled by trade-offs between the cost of producing roots and benefits in nutrient uptake by roots. Here, root development is hypothesized to be a trade-off between root production and environmental limits.

When we compared the two types of sub-models of spatial heterogeneity, the power function-based sub-model generated a better fit than that based on the logistic function. Nevertheless, the latter is more ecologically meaningful and has the potential to be more easily applied to other situations. Once p increases, the two sub-models limit the growth of *RID* in different manners: the power function alone decreased the increment of root density at higher p, while the logistic function gave an asymptote of root density. We suggest using both sub-models for RID estimation, but preferentially choosing the power function for dense forest stands (more likely to have high p) and the logistic function for low-density stands (more likely to have low p). In certain cases, e.g. when calculating the contribution of root systems to hillslope stability (Pollen-Bankhead and Simon, 2009; Schwarz *et al.*, 2010), it is safer to underestimate root density so that the evaluation of slope stability is more conservative. In such a case, preferring a logistic function, which tends to saturate much faster (at approximately p = 0·15), would be more suitable.

The polygon method we developed in the sub-model of spatial heterogeneity differs from the methods used to estimate root density developed by Roering *et al.* (2003) and Müller and Wagner (2003). In the method of Roering *et al.* (2003), root extension of a tree was considered to be a circle and the total root

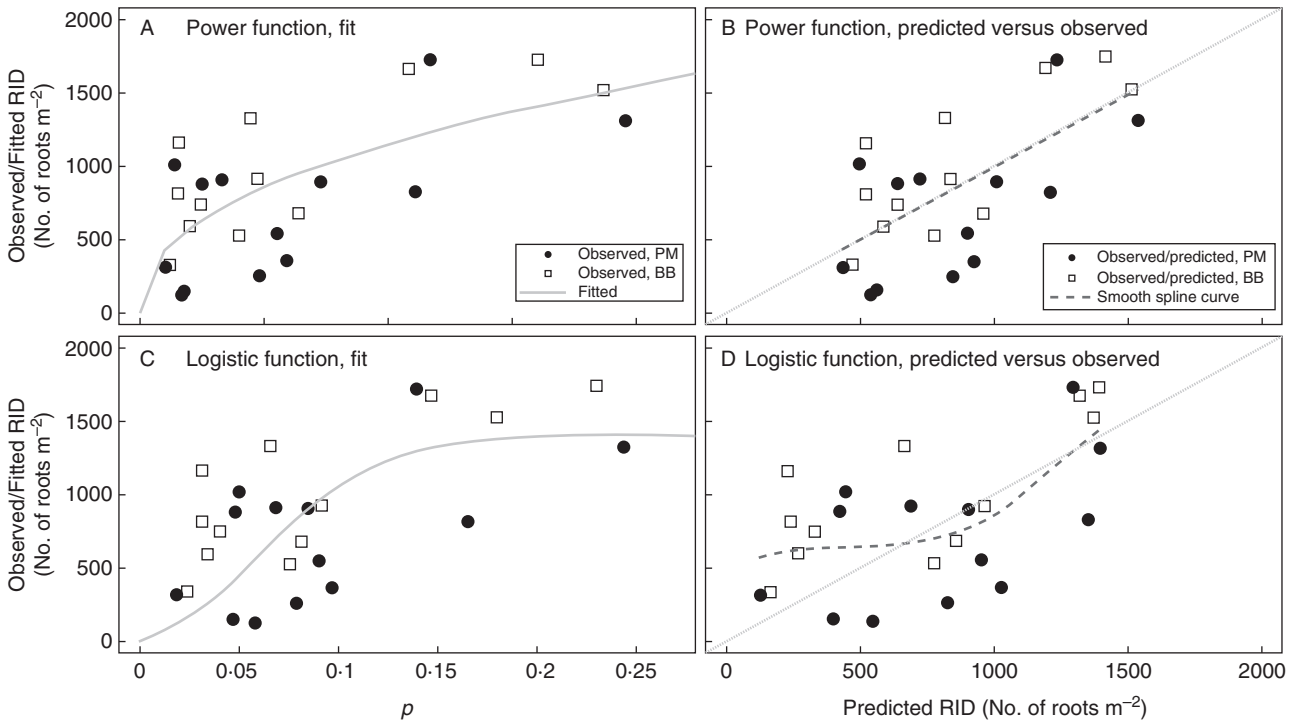

FIG. 5. Fit of the two ultimately selected sub-models of spatial heterogeneity to the observed data. More details about the model comparison are available in Supplementary Data S3. p is the tree root potential. Note that the metric p differs according to the modelling approaches because of the parameter values of λ_s and α (Table 2).

TABLE 2. *Coefficient estimate sub-model of spatial heterogeneity for the two ultimately selected sub-models of spatial heterogeneity*

No. of sub-model	Type of function	Coefficient	Estimate	Standard error	*t*-value
2	Power	λ_a	1·176	0·239	4·933***
		α	1·809	0·390	4·641***
		m	3097·167	1064·776	2·909**
		n	0·429	0·179	2·394*
10	Logistic	λ_a	1·005	0·105	9·565***
		α	1·567	0·214	7·318***
		r	24·608	9·978	2·466*
		K_t	1399·487	228·681	6·120***

The number of each sub-model corresponds to that in Supplementary Data S3.

Both sub-models were fitted for the case when MIZ = 8·0 m and the effect of obstacle was not considered.

***$P < 0·001$; **$P < 0·01$; *$P < 0·05$.

impact of surrounding trees on an oval-shaped landslide scarp (i.e. a surface instead of a point) was the sum of each tree's impact, which varied as a function of tree size and distance. The method of Müller and Wagner (2003) consisted of sampling roots using cores from the centre of a tree gap to its edge (usually the first tree at the border of the gap), rendering a pattern resembling spokes around the gap centre. Our model is more refined because it introduces more precise tree selection criteria, as well as new factors, such as the effect of species, and the interactions between trees and understorey vegetation.

Spatial heterogeneity: abiotic and biotic factors

The effects of both obstacle and competition between trees and understorey species (θ) were considered in the sub-model of spatial heterogeneity, but neither increased the significance or improved the model's fit. We speculate that the null effect of O may be dependent on our data, in which <30 % of mini-monoliths encountered obstacles (mainly at Bachat-Bouloud forest, occasionally at Prémol). Overall, although both θ and O had a null effect in our case studies, we suggest avoiding generalizations and testing these factors when using our model with data from other sites.

Comparisons between the different forms of the sub-model of spatial heterogeneity suggested retaining MIZ = 8·0 m. MIZ should be equal or slightly inferior to the maximum extension radius (MER) of the root system of trees. Schwarz *et al*. (2010) found that a *P. abies* with DBH 30 cm had an MER of ~5·5 m. Ammer (2000, cited by Ammer and Wagner, 2005) proposed 10·0 m as the MER for a *P. abies* of 60 cm DBH. The MER of *P. abies* roots may even reach 12 m, as found by Laitakari (1929). A meta-analysis performed by Day *et al*. (2010) showed that the MER of *P. abies* reached an asymptote of around 6·0 m when DBH was 25–30 cm. As *P. abies* possesses a plate-like root system, it may have had a wider lateral root extension than a tree of similar size in the other species examined in this meta-analysis. The remaining species had either heart or taproot systems. At our sites, 75 % of trees had a DBH <30 cm and only two trees possessed a DBH >60 cm. Therefore, choosing MIZ = 8·0 m appears to be suitable when using data from the literature and was also appropriate for the specific

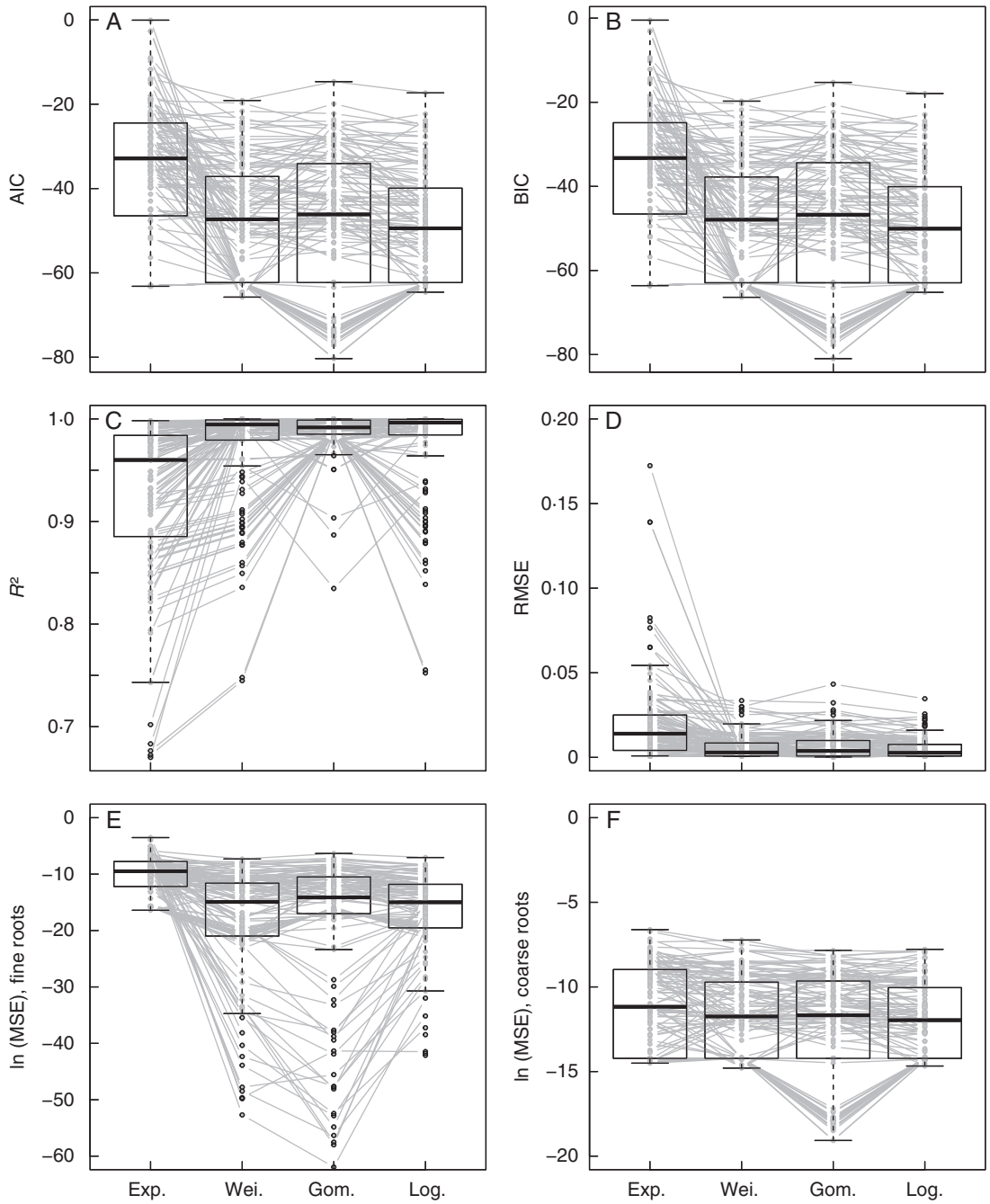

FIG. 6. Comparison of fits between the sub-models of diameter spectrums in terms of the choice of function. Each grey line shows the tendency of the effect of the choice of functions on the same data set.

characteristics of our field site. An alternative approach for selecting trees is angle count sampling, based on the use of a relascope (Schreuder, 1993). Such an approach, which is mostly used to estimate tree basal area in forest stands, requires choosing a limiting angle that defines the maximum distance within which a tree influences a point. Compared with MIZ, such a method may potentially include trees far away from the target point as well as excluding smaller but very close trees. The MIZ approach can, nevertheless, be used in conjunction with angle count sampling to explore the relationship between the surface area of visible trees and that of the stand.

We found that RSA depended significantly on species for the two selected forms of the sub-model of spatial heterogeneity, but fitted λ_s values were only slightly superior to 1·0. This result suggests that the effect of the plate-like root system of *P. abies* was only slightly greater than that of the other species. Therefore, in heterogeneous mountain forest stands, tree position and size influence root density more, compared with

TABLE 3. *Distribution of the best fitted sub-models of root diameter spectrum with regard to the four functions*

Soil depth	Data for fitting	Total no. of equations	Zone I: lowest global MSE				Zone II: lowest MSE of fine roots			Zone III: lowest MSE of coarse roots		
			Exponential	Weibull	Gompertz	Log normal	Weibull	Gompertz	Log normal	Weibull	Gompertz	Log normal
]0·0, 0·2] m	Mini-monolith	25	0	2	2	21	4	4	17	1	8	16
]0·2, 0·4] m	Root trench	24	0	2	7	15	6	12	6	3	6	15
]0·4, 0·6] m	Root trench	24	0	5	3	16	10	11	3	4	5	15
]0·6, 0·8] m	Root trench	24	0	6	7	11	13	8	3	4	8	12
]0·8, 1·0] m	Root trench	24	0	3	18	3	20	2	2	2	18	4

Unit: number (No.) of equations.
Within each group (the three or four values in the same line and the same zone), the highest number of equations is underlined.
When the MSE is decomposed into fine roots (Zone II) and coarse roots (Zone III), only the three two-parameter functions (i.e. Weibull, Gompertz and log-normal CDFs) are compared.

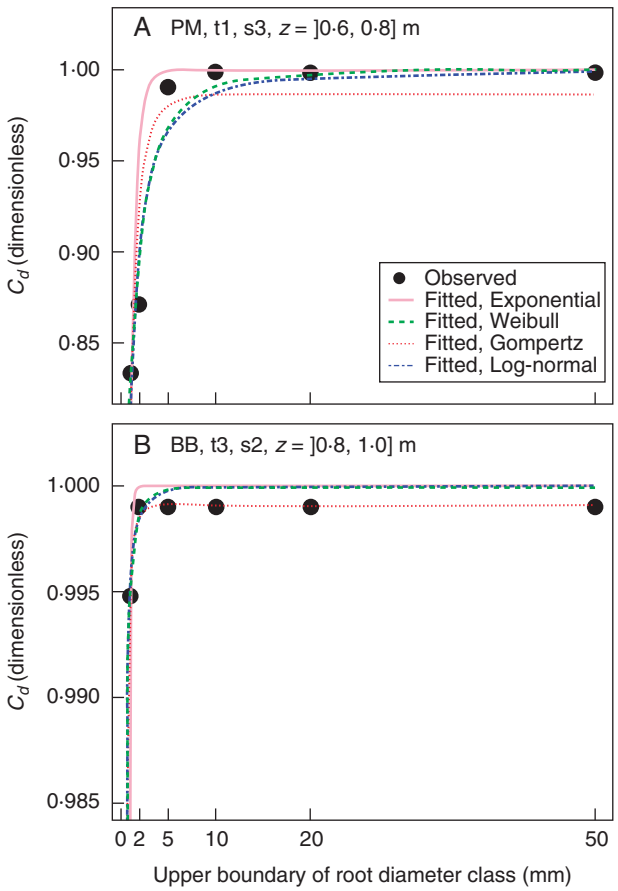

FIG. 7. Two cases of fit of root diameter spectrum using four types of function. Note the different graduation of the *y*-axis in (A) and (B). In this study, the maximum cumulative relative RID was set to 0·999 instead of 1·000, as we were not certain whether the maximum sampled root diameter class]20, 50] mm was the maximum in reality. The log-normal and the Gompertz CDF achieved the best fit in (A) and (B), respectively.

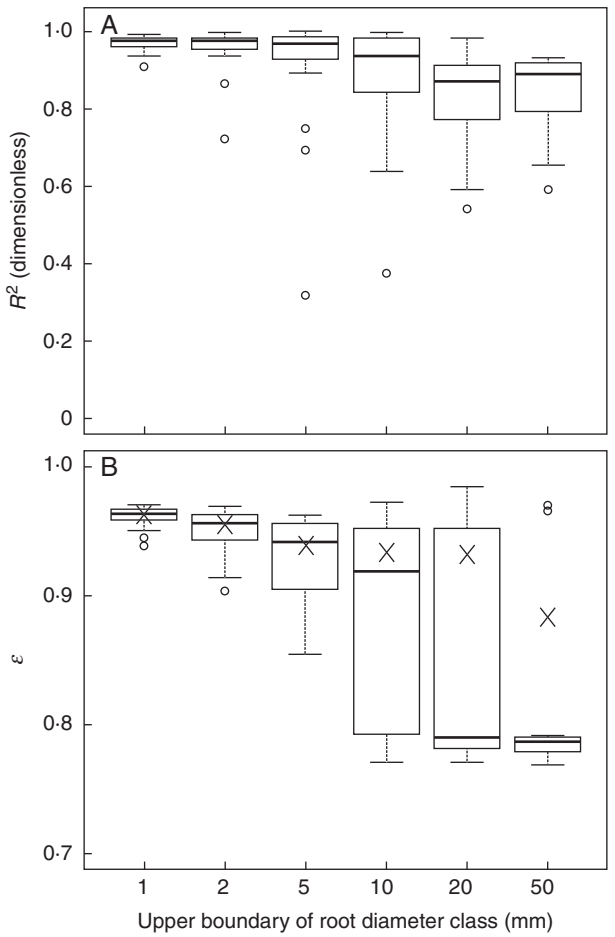

FIG. 8. Fit comparisons of the sub-models of vertical profile between different classes of root diameter. Boxplots in (A) and (B) show the quantiles of R^2 and ε of the one-curve-per-replicate fits, respectively ($N_f = 24$). In (B), crosses denote the value of ε for the global fits to all the root data within one diameter class; hollow points denote outliers. ε is the coefficient of the root profile shape. The closer ε approaches 1, the more the roots tend to be less concentrated at the soil surface.

species and obstacles, especially when the distance between trees is great.

Our data points remained dispersed regardless of the type of function used, especially at lower *p*. This result might be attributed to the effect of site (Prémol versus Bachat-Bouloud), which is not an effect that could be fully investigated in the modelling process. The most distinct difference between the Prémol and Bachat-Bouloud sites concerns relative densities and proportions of species, i.e. there were more *P. abies* and almost no *F. sylvatica* at Bachat-Bouloud, and total stem density

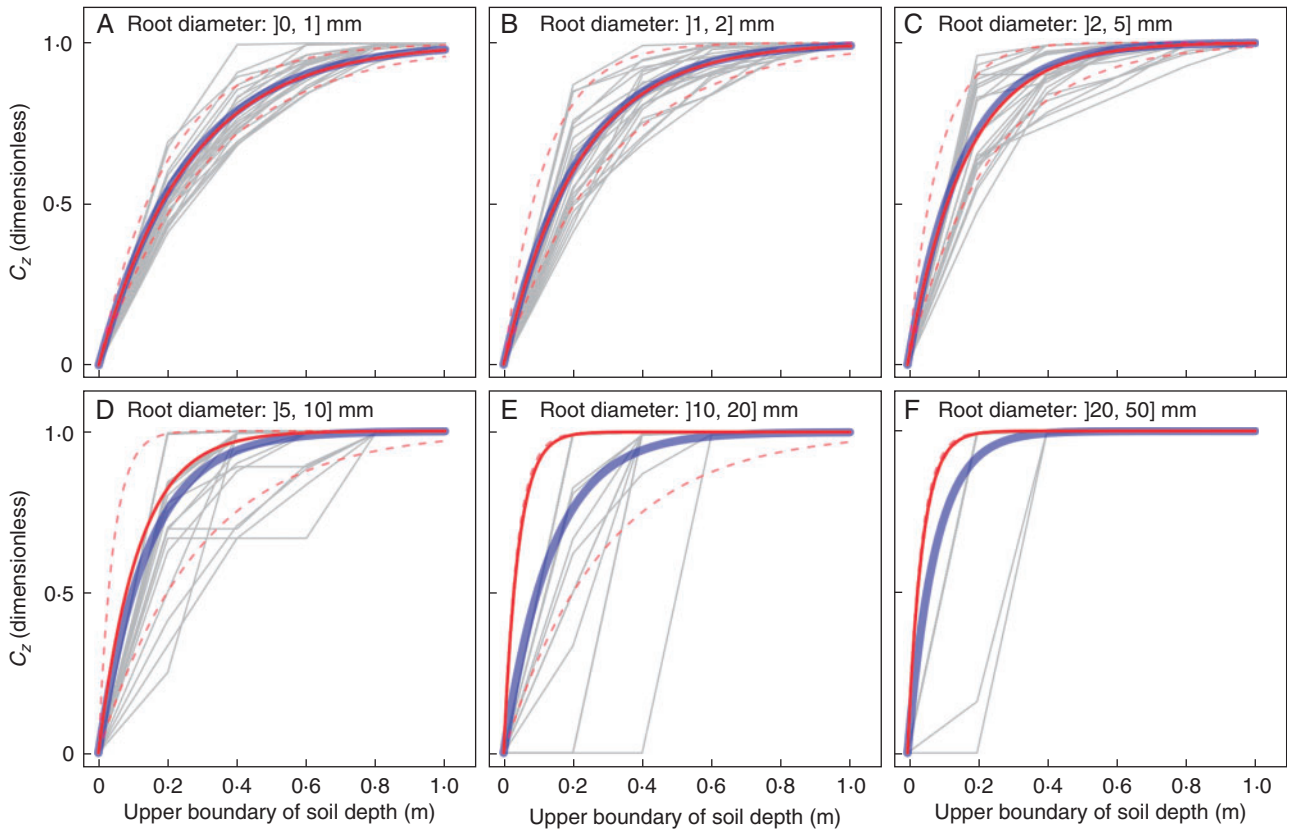

FIG. 9. Fitted (coloured curves) and observed (grey curves) values for the sub-model of vertical profile for different classes of root diameter. In each figure, there are four tracked fitted curves, including one global fit to all the root data within one diameter class (thick solid curve in blue) and three local one-curve-per-replicate fits ($N_f = 24$): the 10th quantile (upper thin dashed curve in red), median (medium solid curve in red) and 90th quantile (lower thin dashed curve in red) of ε.

at Prémol was higher. In ChaMRoots, the effect of site was interpreted by the effect of species, root architecture and tree distance. Nevertheless, Bachat-Bouloud tended to have a higher baseline of RID compared with Prémol. This trend could be attributed to the soil fertility in shallow soil layers, as Bachat-Bouloud possessed a thicker humus layer than Prémol, potentially providing nutrients for maintaining root growth (Vanninen and Mäkelä 1999). Confirming such an effect would require the investigation of more sites along a forest productivity gradient in this region.

Diameter spectrum

Empirically, past studies have used non-linear and low-parameter distributions to model diameter spectrum, e.g. power, exponential, Rayleigh, normal, logistic, Weibull, log-normal and bimodal distributions (Anderson *et al.*, 2007; Pollen-Bankhead and Simon, 2009; Scanlan and Hinz, 2010; Schwarz *et al.*, 2010; Cohen *et al.*, 2011). Results from these different models cannot be compared due to the disparity in species investigated and the use of different root diameter classes. For example, Anderson *et al.* (2007) proposed six-parameter bimodal functions instead of unimodal functions for the non-cumulative density of grass roots, because the interval of root diameter class was very small (0·064 mm). By using 0·2 mm as an interval of root diameter class, Scanlan and Hinz (2010) fitted a cumulative relative density for grass roots of]0, 2] mm in diameter and found that log-normal and Weibull distributions resulted in better fits than exponential, Rayleigh, normal and logistic functions. Therefore, we adopted the following thresholds to split root diameter: 1, 2, (3), 5, 10 and 20 mm; these are frequently used for tree species (Hoffmann and Usoltsev, 2001). These heterogeneous root diameter classes can raise difficulties in modelling diameter spectrums because RID can be over-dispersed at large diameter values. This problem was not the case in our study as all the selected two-parameter CDFs provided satisfactory fits. Simultaneously, we found that the Gompertz and log-normal CDFs had complementary advantages in fitting data. The Gompertz CDF performed better in modelling angular shoulder and shoulderless diameter spectrums. This feature could be associated with its double exponential structure, which makes the curve increase rapidly to the maximum. The Gompertz model, which has been successfully applied in life sciences for modelling human mortality (Gompertz, 1825) and tumour growth (Laird, 1964), has thus also demonstrated strong potential for modelling root distributions.

Our results showed that the evolution of diameter spectrum was more vertical than horizontal, as soil depth significantly impacted diameter spectrum, but p did not. Soil depth also affected the choice of CDF by modifying the shape of the diameter spectrum, demonstrating its importance. No significant effect of p was found on the parameters in the diameter spectrum, suggesting that the spectrum varied independently of

above-ground tree positions and size. Thus, a generic equation could be used for mountain forest sites in the future.

Vertical profile

The one-parameter exponential model of Gale and Grigal (1987) facilitates comparisons between sites and studies due to its unique coefficient. However, the model fit or prediction can be significantly biased if root excavation does not attain the maximum rooting depth. Our sub-model of vertical profile for modelling the cumulative root density is slightly different from the model of Gale and Grigal (1987) due to the term z_{max}. This term ensures that the value of the index varies between 0 and 100. We think that it is extremely important to estimate z_{max} when modelling cumulative root density, because otherwise it would not be possible to determine at which soil depth C_z attains 1·0.

Many studies have adopted the one-parameter exponential model for modelling cumulative root density at a continental scale (e.g. Jackson *et al*., 1996; Smart *et al*., 2006; Tao *et al*., 2009) and at local site scales (e.g. King *et al*., 2003; Moreno *et al*., 2005; Pollen-Bankhead and Simon, 2009; Meinen *et al*., 2009). Previous studies seldom investigated the effect of root diameter when characterizing or modelling vertical profiles, or they fitted a global curve for all roots. We found that root diameter significantly affected the vertical profile and that coarser roots were more concentrated in shallow soil layers. This result highlights the importance of taking into account root diameter in vertical profile modelling. Simultaneously, our results challenged the relevance of applying the model of Gale and Grigal (1987) at a local site scale, as our vertical profile showed drastically different shape variations at this local scale within and between root diameter classes. Moreover, the model fit tended to be poorer with increasing root diameter, suggesting the less appropriate use of one parameter models (Gale and Grigal, 1987) for very coarse roots (diameter >5 mm). This result was probably obtained because larger roots may have a more heterogeneous distribution due to their greater size and lower quantity in a population. Testing the relevance of using multiple-parameter functions for modelling a vertical profile is therefore of great interest for future studies.

Vertical profiles of plant roots can be significantly affected by functional groups (Jackson *et al*., 1996) or species (Kalliokoski, 2011). We showed that the effect of species on the vertical profile parameter ε could not be tested directly because the forest stands were mixed, but was included in tree potential p and the effect of site. The value of ε was only significantly different with regard to the site factor. However, this significant effect might be due to multiple reasons, e.g. species composition, tree density, and also soil properties either linked to sites themselves or a consequence of mixture of species (Rothe and Binkley, 2001). Therefore, more factors concerning species and soil characteristics should be considered in future studies in order to better explain the variation of ε.

Global structure of ChaMRoots

By combining the three sub-models of ChaMRoots, RID per class of diameter and per soil layer can be predicted. Theoretically, the algorithm used for the sub-model of spatial heterogeneity could have been applied to any class of diameter at any soil layer. The 'three sub-models' pattern is more adapted than the 'one sub-model of spatial heterogeneity for all' pattern for two reasons. Firstly, in our RID data, only the relationship between $RID_{t,0-1}$ of the upper soil layer and p was highly sensitive and thus feasible for root density prediction. This result was also found by Roberts (1976), who showed that the distance-dependent relationship was uniquely sensitive to the finest roots. Nevertheless, according to Vanninen and Mäkelä (1999), who investigated root density of *Pinus sylvestris*, it is more difficult to achieve a good allometric relationship with above-ground stand characteristics for very fine roots (]0, 2] mm) than for coarser roots (]2, 5] mm). This controversial point about the feasibility of modelling fine and coarse roots deserves further exploration. Besides, the 'three sub-models' pattern possessed significantly fewer parameters and thus was easier to calibrate. The 'three sub-models' approach connects and keeps each process (spatial heterogeneity, diameter spectrum and vertical profile) relatively independent, with potential future independent updates.

Limits and perspectives

Slope angle is an important factor affecting root distribution (Di Iorio *et al*., 2005; Chiatante and Scippa, 2006) and this might be particularly true for mountain forests with complex topography. Nevertheless, considering the effect of slope would make it necessary to take into account several factors associated with slope, including site exposition, location of the tree trunk (upslope/downslope), and position along a slope (crest, middle, toe, as this influences soil depth), thus rendering the modelling and root sampling work more complex. As this study was the first step towards modelling root distributions based on the concept of tree root potential, the effect of slope was not considered. Accordingly, our root sampling was conducted on gentle slopes (mostly <10°). With increasing interest in modelling root distribution along steeper slopes (≥20°), the impact of slope on root distribution will be explored on the basis of the existing model structure. For example, it could be feasible to weight the contribution of each tree to p by introducing parameters associated with slope angle and location of the tree trunk.

The growth of roots and their spatial distribution can also be affected by several edaphic factors [e.g. water and nutrient availability in soil, texture and compaction level (Coutts *et al*., 1999; Dexter, 2004)]. These factors may be spatially heterogeneous, thus resulting in patchiness. The current version of ChaMRoots can predict the gradient of root distribution in space, but cannot account for resource patchiness. Incorporating edaphic factors might thus be necessary for a more refined prediction at local scales. Nevertheless, extra soil parameters would also increase the number and cost of measurements as well as the complexity of the model. The choice of parameters for the model should be adapted according to the precision required.

Root grafting, defined as the functional union of two or several roots subsequent to their formation, occurs in many tree species, including *P. abies* (Külla and Lõhmus, 1999). Such a phenomenon is not considered by ChaMRoots, as we counted

root tips without identifying whether a root was grafted or not. A better understanding of the mechanism and distribution of root grafting is primarily desired for heterogeneous mountain forests before it can be considered by models of root distribution.

ChaMRoots cannot predict the exact quantity of trees contributing to root density, but aims to include trees that significantly contribute to tree root potential (p). Determining the number of trees whose roots are present at a given point is therefore an important issue. Combining both *in situ* root excavation and molecular techniques to identify species would be highly useful to address this issue.

In our study, the data for model calibration and validation were obtained in the same plots. It would be useful to validate the model using ground truth data from other plots or even other types of forest. Unfortunately, data separating both tree and understorey species' roots and tree coordinates and dendrometric characteristics remain very scanty. Our mini-monolith techniques designed for this use should therefore be applied to other sites to improve model validation.

Conclusions

The majority of published root models have been developed at the scale of the plant individual. These models are in general not suitable for modelling the spatial distribution of root density for highly heterogeneous forests with regard to both species and environment. Alternatively, our semi-mechanistic model, ChaMRoots, focuses on the spatial distribution of root density at the tree cluster scale. Based on easy-to-measure characteristics, simple forest inventory protocols and three sub-models, we achieved a good compromise between the complexity of the case study area and that of the global model structure. Overall, ChaMRoots was a powerful tool for simulating root distribution at the scale of the forest ecosystem. In terms of model principles, structure and algorithms, ChaMRoots can be considered complementary to the state-of-art of modelling of root spatial distribution.

SUPPLEMENTARY DATA

Supplementary data are available online at www.aob.oxfordjournals.org and consist of the following. S1: derivation of the logistic function-based sub-model Spatial Heterogeneity in ChaMRoots. S2: protocol for selecting visible trees and outcomes of the application to the forest data collected from the French Alps. S3: supplementary table and figures giving details of model comparison, correlation between coefficients and model validation.

ACKNOWLEDGEMENTS

This study was financed by ARANGE project (FP7 Theme KBBE. 2011.1.2-07). The UR BEF is supported by the French National Research Agency through the Laboratory of Excellence ARBRE (ANR-11-LABX-0002-01) and the project QLSPIMS. We thank ONF and Chamrousse Mairie for their authorization of root sampling and support in site selection. We are grateful to many colleagues for their help with field and laboratory work and logistics: B. Courbaud (IRSTEA), Lu Feng (CIRAD), M. Foulonneau (USMB), C. Gadenne (AgroParisTech), M. Genet (INRA), H. Géraud (CIRAD), C. Jourdan (CIRAD), F.-X. Mine (ISARA), J. Nespoulous (INRA) and H. Rey (CIRAD). Finally, we thank H. Vogt-Schilb (WOAINI), Huaxiang Zhu (IRSTEA) and Wentao Chen (UGA) for their inspiring comments throughout the modelling study.

LITERATURE CITED

Ammer C. 2000. *Untersuchungen zum Einfluss von Fichtenaltbeständen auf die Entwicklung junger Buchen*. Aachen: Shaker.

Ammer C, Wagner S. 2002. Problems and options in modelling fine root biomass of single mature Norway spruce trees at given points from stand data. *Canadian Journal of Forest Research* **32**: 581–590.

Ammer C, Wagner S. 2005. An approach for modelling the mean fine-root biomass of Norway spruce stands. *Trees: Structure and Function* **19**: 145–153.

Anderson T, Starmer W, Thorne M. 2007. Bimodal root diameter distributions in Serengeti grasses exhibit plasticity in response to defoliation and soil texture: implications for nitrogen uptake. *Functional Ecology* **21**: 50–60.

Böhm W. 1979. *Methods of studying root systems*. Berlin: Springer.

Burnham KP, Anderson DR. 2002. *Model selection and multimodel inference: a practical information-theoretic approach*, 2nd edn. New York: Springer.

Cardinael R, Mao Z, Prieto I, *et al.* 2015. Competition with winter crops induces deeper rooting of walnut trees in a Mediterranean alley cropping agroforestry system. *Plant and Soil* **391**: 219–235.

Chiatante D, Scippa GS. 2006. Root architecture: influence of metameric organization and emission. *Plant Biosystems* **140**: 307–320.

Chopart JL, Rodrigues S, de Azevedo MC, Medina CD. 2008. Estimating sugarcane root length density through root mapping and orientation modelling. *Plant and Soil* **313**: 101–112.

Cohen D, Schwarz M, Or D. 2011. An analytical fiber bundle model for pullout mechanics of root bundles. *Journal of Geophysical Research: Earth Surface* **116** (F3) doi:10.1029/2010JF001886.

Coleman M. 2007. Spatial and temporal patterns of root distribution in developing stands of four woody crop species grown with drip irrigation and fertilization. *Plant and Soil* **299**: 195–213.

Collet C, Löf M, Pagès L. 2006. Root system development of oak seedlings analysed using an architectural model. Effects of competition with grass. *Plant and Soil* **279**: 367–383.

Coutts MP. 1983. Root architecture and tree stability. *Plant and Soil* **71**: 171−188.

Coutts MP, Nielsen CNN, Nicoll BC. 1999. The development of symmetry, rigidity and anchorage in the structural root system of conifers. *Plant and Soil* **217**: 1–15.

Day SD, Wiseman PE, Dickinson SB, Harris JR. 2010. Contemporary concepts of root system architecture of urban trees. *Arboriculture & Urban Forestry* **36**: 149–159.

Dexter AR. 2004. Soil physical quality: part I. Theory, effects of soil texture, density, and organic matter, and effects on root growth. *Geoderma* **120**: 201–214.

Doussan C, Pagès L, Pierret A. 2003. Soil exploration and resource acquisition by plant roots: an architectural and modelling point of view. *Agronomie* **23**: 419–431.

Gale MR, Grigal DF. 1987. Vertical root distributions of northern tree species in relation to successional status. *Canadian Journal of Forest Research* **17**: 829–834.

Gao Y, Duan A, Qiu X, *et al.* 2010. Distribution of roots and root length density in a maize/soybean strip intercropping system. *Agricultural Water Management* **98**: 199–212.

Gersani M, O'Brien EE, Maina GM, Abramsky Z. 2001. Tragedy of the commons as a result of root competition. *Journal of Ecology* **89**: 660–669.

Gompertz B. 1825. On the nature of the function expressive of the law of human mortality, and on a new mode of determining the value of life contingencies. *Philosophical Transactions of the Royal Society of London* **115**: 513–583.

Hertel, D, Schöling, D. 2011. Below-ground response of Norway spruce to climate conditions at Mt. Brocken (Germany)—A re-assessment of Central Europe's northernmost treeline. *Flora* **206**:127–135.

Hoffmann CW, Usoltsev VA. 2001. Modelling root biomass distribution in *Pinus sylvestris* forests of the Turgai Depression of Kazakhstan. *Forest Ecology and Management* **149**: 103–114.

Di Iorio A. Lasserre B, Scippa GS, Chiatante D. 2005. Root system architecture of *Quercus pubescens* trees growing on different sloping conditions. *Annals of Botany* **95**: 351–361.

IUSS Working Group WRB, 2007. *World reference base for soil resources 2006, first update 2007. World Soil Resources Reports No. 103*. Rome: FAO.

Jackson RB, Canadell J, Ehleringer JR, Mooney HA, Sala OE, Schulze ED. 1996. A global analysis of root distributions for terrestrial biomes. *Oecologia* **108**: 389–411.

Kalliokoski T. 2011. *Root system traits of Norway spruce, Scots pine, and silver birch in mixed boreal forests: an analysis of root architecture, morphology, and anatomy*. PhD Thesis, Department of Forest Sciences, Faculty of Agriculture and Forestry, University of Helsinki.

King J, Gay A, Sylvester-Bradley R, *et al.* 2003. Modelling cereal root systems for water and nitrogen capture: towards an economic optimum. *Annals of Botany* **91**: 383–390.

Köstler JN, Brückner E, Bibelriether H. 1968. *Die Wurzeln der Waldbäume. Untersuchungen zur Morphologie der Waldbaume in Mitteleuropa*. Verlag Paul Parey: Hamburg & Berlin **284**: 3–4.

Külla T, Lõhmus K. 1999. Influence of cultivation method on root grafting in Norway spruce (*Picea abies* (L.) Karst.). *Plant and Soil* **207**: 91–100.

Laird, AK. 1964. Dynamics of tumor growth. *British Journal of Cancer* **18**,: 490–502.

Laitakari E. 1929. Männyn juuristo. Morfologinen tutkimus. *Acta Forestalla Fennica* **33**: 1–380.

Mao Z, Saint-André L, Genet M, *et al.* 2012. Engineering ecological protection against landslides in diverse mountain forests: choosing cohesion models. *Ecological Engineering* **45**: 55–69.

Mao Z, Jourdan C, Bonis ML, *et al.* 2013. Modelling root demography in heterogeneous mountain forests and applications for slope stability analysis. *Plant and Soil* **363**: 357–382.

Mao Z, Wang Y, Cécillon L, *et al.* 2015. Characterising above- and below-ground carbon partitioning in forest trees along an altitudinal gradient using area-based indicators. *Arctic, Antarctic, and Alpine Research* **47**: 59–69.

Maurice J, Laclau JP, Re DS, *et al.* 2010. Fine root anisotropy in *Eucalyptus grandis* plantations. Towards the prediction of root length densities from root counts on trench walls. *Plant and Soil* **334**: 261–275.

Meinen C, Leuschner C, Ryan NT, Hertel D. 2009. No evidence of spatial root system segregation and elevated fine root biomass in multi-species temperate broad-leaved forests. *Trees: Structure and Function* **23**: 941–950.

Moreno G, Obrador JJ, Cubera E, Dupraz C. 2005. Fine root distribution in Dehesas of central-western Spain. *Plant and Soil* **277**: 153–162.

Mulia R, Dupraz C, van Noordwijk M. 2010. Reconciling root plasticity and architectural ground rules in tree root growth models with voxel automata. *Plant and Soil* **337**: 77–92.

Müller K, Wagner S. 2003. Fine-root dynamics in gaps of Norway spruce stands in the Germany Ore mountains. *Forestry* **76**: 149–158.

van Noordwijk M, Lawson G, Soumaré A, Groot JJR, Hairiah K. 1996. Root distribution of trees and crops: competition and/or complementary. In: CK Ong, P Huxley, eds. *Tree-crop interactions*. Wallingford: CAB International, 319–363.

O'Brien EE, Brown JS, Moll JD. 2007. Roots in space: a spatially explicit model for below-ground competition in plants. *Proceedings of the Royal Society of London B: Biological Sciences* **274**: 929–935.

Pagès L, Vercambre G, Drouet JL, Lecompte F, Collet C, Le Bot J. 2004. Root Typ: a generic model to depict and analyse the root system architecture. *Plant and Soil* **258**: 103–119.

Picard N, Saint-André L, Henry M. 2012. *Manual for building tree volume and biomass allometric equations: from field measurement to prediction*. Rome: Food and Agricultural Organization of the United Nations; Montpellier: Centre de Coopération Internationale en Recherche Agronomique pour le Développement.

Pollen-Bankhead N, Simon A. 2009. Enhanced application of root-reinforcement algorithms for bank-stability modeling. *Earth Surface Processes and Landforms* **480**: 471–480.

Roberts J. 1976. A study of root distribution and growth in a *Pinus sylvestris* L. (Scots pine) plantation in East Anglia. *Plant and Soil* **44**: 607–621.

Roering JJ, Schmidt KM, Stock JD, Dietrich WE, Montgomery DR. 2003. Shallow landsliding, root reinforcement, and the spatial distribution of trees in the Oregon Coast Range. *Canadian Geotechnical Journal* **40**: 237–253.

Rothe A, Binkley D, 2001. Nutritional interactions in mixed species forests: a synthesis. *Canadian Journal of Forest Research* **31**: 1855–1870.

Scanlan CA, Hinz C. 2010. Using radius frequency distribution functions as a metric for quantifying root systems - root radius frequency distributions. *Plant and Soil* **332**: 475–493.

Schenk HJ, Jackson RB. 2002. Rooting depths, lateral root spreads and below-ground/above-ground allometries of plants in water-limited ecosystems. *Journal of Ecology* **90**: 480–494.

Schreuder HT. 1993. *Sampling methods for multiresource forest inventory*. New York: Wiley.

Schwarz M, Lehmann P, Or D. 2010. Quantifying lateral root reinforcement in steep slopes – from a bundle of roots to tree stands. *Earth Surface Processes and Landforms* **35**: 354–367.

Smart DR, Schwass E, Lakso A, Morano L. 2006. Grapevine rooting patterns: a comprehensive analysis and a review. *American Journal of Enology and Viticulture* **57**: 89–104.

Soethe N, Lehmann J, Engels C. 2006. Root morphology and anchorage of six native tree species from a tropical montane forest and an elfin forest in Ecuador. *Plant and Soil* **279**: 173–185.

Stokes A, Atger C, Bengough AG, Fourcaud T, Sidle RC. 2009. Desirable plant root traits for protecting natural and engineered slopes against landslides. *Plant and Soil* **324**: 1–30.

Tao F, Yokozawa M, Zhang Z. 2009. Modelling the impacts of weather and climate variability on crop productivity over a large area: a new process-based model development, optimization, and uncertainties analysis. *Agricultural and Forest Meteorology* **149**: 831–850.

van Noordwijk M, Brouwer G, Meijboom F, do Rosario G, Oliveira M, Bengough AG. 2000. Trench profile techniques and core break methods. In: AL Smit, AG Bengough, C Engels, M Van Noordwijk, S Pellerin, Van der Geijn, eds. *Root methods: a handbook*. Berlin: Springer, 211–233.

Vanninen P, Mäkelä A. 1999. Fine root biomass of Scots pine stands differing in age and soil fertility in southern Finland. *Tree Physiology* **19**: 823–830.

Vogt KA, Vogt DJ, Palmiotto PA, Boon P, O'Hara J, Asbjornsen H. 1996. Review of root dynamics in forest ecosystems grouped by climate, climatic forest type and species. *Plant and Soil* **187**: 159–219.

Zianis D, Muukkonen P, Mäkipää R, Mencuccini M. 2005. Biomass and stem volume equations for tree species in Europe. *Silva Fennica Monographs*, Vol. 4.

APPENDIX

Abbreviations and symbols

Name	Meaning
Abbreviations used in the text	
AIC	Akaike information criterion
ARB	Allometric relationship-based (model)
BIC	Bayesian information criterion
CDF	Cumulative distribution function
DBH	Tree stem diameter at breast height (1·30 m)
MER	Maximum extension radius
MIZ	Maximum root inclusion zone
MSE	Mean square error
RID	Root interception density

(Continued)

Continued

Name	Meaning
RLD	Root length density
RSA	Root system architecture
RMSE	Root mean square error
Expressions used in equations	
a	Slope of the linear correlation between $RID_{t,1-5}$ and $RID_{t,0-1}$
b	Intercept of the linear correlation between $RID_{t,1-5}$ and $RID_{t,0-1}$
C_d	Cumulative frequency of root interception density from the finest roots to those of class of root diameter d mm (dimensionless)
C_z	Cumulative frequency of RID from ground surface to the soil depth z (dimensionless)
D_i	Horizontal distance from the tree centre to the target point (m)
d	Upper boundary of root diameter class (mm)
E	Production efficiency (no. of roots / potential of trees to grow roots at a given point in the soil)
e	Subscript standing for a tree individual e
g	Basal area of tree i at height 1·3 m (m^2)
K	Maximum RID_{0-1} of both tree and understorey species that the soil can support
K_t	Maximum RID_{0-1} of tree roots that the soil can support
k	Number of parameters in the model
L	Maximized value of the likelihood function for the estimated model
m	Coefficient of the power function, sub-model of spatial heterogeneity
N_e	Number of effective trees around the target point (number of trees)
N_f, N_v	Number of dataset used for model fitting and crossed validation and validation, respectively
N_{inside}, N_{outside}	Number of mini-monoliths situated inside and outside of tree canopies, respectively
N_o	Number of observations within each model fit
N_s	Number of tree species
n	Coefficient of the power function, sub-model of spatial heterogeneity; when it occurs as a subscript it stands for sequence of mini-monolith
O_i	Absence of emerged obstacles on the ground between the target point and tree i, either binary (1, 0) or unique (0) value (dimensionless)
P_t, P_u	Percentage of root density of tree and understorey species in total root density (%)
P_{TI}, P_G	Percentage of root density from tree species at tree islands and gaps (%)
p	Metric describing the potential of trees to grow roots at a given point in the soil. The term 'tree root potential' will be used below.
p_i, $p_{i,s}$	Tree root potential of tree i or tree i of species s
p_p, p_a, p_b	Tree root potential of *Picea abies*, *Abies alba* and broadleaves (mainly composed of *Fagus sylvatica*)
p_s	Generic symbol standing for p_p, p_a, p_b (subscript s denotes species p, a or b)
R^2	Coefficient of determination (dimensionless)
$RID_{t,x-y}$	Measured root interception density of tree roots in the class of root diameter]x, y] mm.
$RID_{t,0-1}$, $\widehat{RID_{t,0-1}}$	Measured and estimated root interception density of tree species of the diameter class]0, 1] mm
$RID_{u,0-1}$, $\widehat{RID_{u,0-1}}$	Measured and estimated root interception density of understorey species of diameter class]0, 1] mm
$RLD_{t,0-1}$, $RLD_{u,0-1}$	Measured root length density of tree and understorey species of diameter class]0, 1] mm
r	Average branching rate for the production of RID_{0-1}
s	Subscript standing for a species
t	Subscript standing for trees
U	Intermediary variable in the logistic function based sub-model of spatial heterogeneity
u	Subscript standing for understorey species
x, y	Lower and upper boundaries of diameter class (mm)
$\widehat{Y}_i$, Y_i	Predicted and observed indicators
z	Upper boundary of depth of soil layer (m)
$z_{\max}$	Maximum soil depth (m)
Symbols used in equations	
α	Coefficient toward D_i to model tree root potential (index), sub-model of spatial heterogeneity
β	Coefficient toward D_i, to model tree root potential (intercept), sub-model of spatial heterogeneity
γ	Coefficient of the Weibull cumulative distribution function (scale), sub-model of diameter spectrum
δ	Coefficient of the Gompertz cumulative distribution function (scale), sub-model of diameter spectrum
ε	Coefficient of the root profile shape, sub-model of vertical profile
ζ	Coefficient of the exponential cumulative distribution function, sub-model of diameter spectrum
η	Coefficient of the Gompertz cumulative distribution function (shape), sub-model of diameter spectrum
θ	Coefficient of competitiveness of understorey species' roots compared with tree roots, sub-model of spatial heterogeneity
κ	Coefficient of the Weibull cumulative distribution function (shape), sub-model of diameter spectrum
λ_p, λ_a, λ_b	Specific coefficients of root potential for *Picea abies*, *Abies alba* and broadleaves (mainly composed of *Fagus sylvatica*), sub-model of spatial heterogeneity
λ_s	Generic symbol standing for λ_p, λ_a, λ_b (the subscript s denotes species p, a or b), sub-model of spatial heterogeneity
μ	Coefficient of the log-normal cumulative distribution function (location), sub-model of diameter spectrum
σ	Coefficient of the log-normal cumulative distribution function (scale), sub-model of diameter spectrum
φ_s	Specific coefficients of root potential for *Picea abies*, *Abies alba* and broadleaves (mainly composed of *Fagus sylvatica*), and the subscript s that denotes species can be p, a or b, sub-model of spatial heterogeneity